Research article

Jinfeng Zhu*, Xizhao Chen, Yinong Xie, Jun-Yu Ou, Huanyang Chen and Qing Huo Liu

Imprinted plasmonic measuring nanocylinders for nanoscale volumes of materials

https://doi.org/10.1515/nanoph-2019-0369
Received September 18, 2019; revised November 3, 2019; accepted November 6, 2019

Abstract: Optical measurement of materials at the nanoscale is important for nanotechnology. Various plasmonic nanorulers have been studied for measuring nanoscale distance and orientation of materials, but they lack the capability to contain and measure nanoscale volumes, especially for liquid or soft materials. Here, we demonstrate the use of imprinted plasmonic volumetric nanocylinders, which act as nanoscale graduated cylinders and facilitate nanomaterial measurement via visible light. Our theoretical and experimental achievements illuminate a promising method for non-destructive, low-cost and fast measurement of material volume changes at the nanoscale, which will benefit the fields of analytical chemistry, nanofabrication and biomedical sensing.

Keywords: plasmonics; nanoimprint lithography; nanocylinders; nanoscale measurement.

1 Introduction

Quantitative analysis on nanoscale volumes of material is critical to a variety of applications on nanotechnology, such as the synthesis of nanocrystals, drug delivery in microsystems, analytical chemistry, physical parameter measurement of nanomaterials, integrated circuit technology, dynamics of nanofluidics and structure biology [1–7]. Therefore, the precise measurement and control of the nanoscale volumes of material are of great interest in the scientific and technological communities. To date, there have been many microscopy methods developed to characterize and measure specimens at the nanoscale [8–10], such as scanning electron microscopy (SEM), atomic force microscopy, environmental SEM, and cryo-electron microscopy. However, these methods usually suffer from destructive operations on the test materials, low measuring speed, and complicated electronic apparatus with high expense. Conventional optical microscopy is a good choice for fast and non-destructive measurement, but it is usually not feasible for measuring nanoscale objects due to light diffraction limits and low optical resolutions. In the past few years, the optical method based on plasmonic effects has demonstrated a promising potential for non-destructive and convenient measurement of nanoscale objects, and a series of plasmonic rulers have been proposed and exploited for measuring nanoscale distance and orientation of biological or soft materials [11–13]. Typically, these plasmonic rulers consist of noble metal nanoparticles (NMNPs) in close proximity or NMNPs with a metallic mirror. For instance, Dathe et al. adopted a plasmonic nanoruler with NMNPs and a flat metallic layer for biomolecule detection [14]; Li et al. used NMNPs on a gold substrate to probe interfacial water structures [15]; some other researchers have also investigated the quantum mechanism for the subnanometer gaps between the plasmonic nanostructures [16, 17]. Despite this, such nanostructures lack the capability to contain and measure nanoscale volumes of materials, especially for liquid or soft materials. With the aim of developing a measuring function for nanoscale volumes of materials, we propose a simple design of plasmonic volumetric nanocylinders based on nanostructured gold, which allows performance with the use of visible light and enables low-cost non-destructive measurement in a fast way. The plasmonic volumetric nanocylinders are analogous to the conventional graduated cylinders in the macroscopic world and adopt a simple visible light spectrometer, which plays the

***Corresponding author: Jinfeng Zhu,** Institute of Electromagnetics and Acoustics, Xiamen University, Xiamen 361005, China; and Shenzhen Research Institute of Xiamen University, Shenzhen 518057, China, e-mail: nanoantenna@hotmail.com.
https://orcid.org/0000-0003-3666-6763
Xizhao Chen, Yinong Xie and Huanyang Chen: Institute of Electromagnetics and Acoustics, Xiamen University, Xiamen 361005, China
Jun-Yu Ou: Optoelectronics Research Centre and Centre for Photonic Metamaterials, University of Southampton, Highfield, Southampton, SO17 1BJ, UK
Qing Huo Liu: Department of Electrical and Computer Engineering, Duke University, Durham, NC 27708, USA

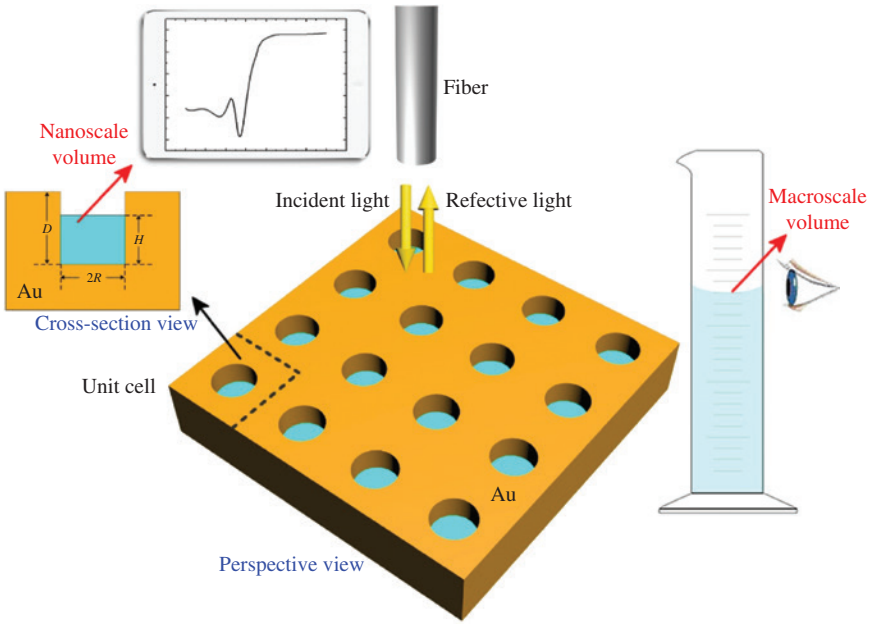

Figure 1: Measurement of nanoscale volumes by gold plasmonic nanocylinders using a fiber spectrometer, where the symbols *D*, *R* and *H* denote the depth and diameter of the nanocylinder, and the height of the specimen.

role of human eyes and "reads" the value of a nanoscale volume. We theoretically estimate the measuring functionality of plasmonic nanocylinders and experimentally demonstrate the measuring sensitivity in the case of loading polystyrene (PS) nanospheres and paraffin.

Our plasmonic measuring tool consists of a gold substrate with periodic volumetric nanocylinders, as illustrated in Figure 1. The geometry of a nanocylinder is described by its radius *R* and depth *D*. In order to simplify the physical model, we assume that the top surface of the specimen with a nanoscale volume is parallel to the surface of the nanocylinder bottom, as shown in Figure 1. In addition, *H* denotes the height of the specimen. The measurement can be performed by applying normal incident light on a certain area of the nanocylinder array with an identical amount of material in each nanocylinder. Based on the spectral shift of plasmonic resonance, one can measure the nanoscale volumes of the loaded materials.

2 Experimental

2.1 Materials and characterization

The water suspension of PS nanosphere (diameter of about 30 nm, size deviation of less than 3%, weight concentration of 5%) is from Huge Biotechnology (Shanghai, China). The ultraviolet (UV) nanoimprint resist TU-170 is from Obducat AB (Lund, Sweden). The paraffin is from Sigma Aldrich (St. Louis, MO, USA). A scanning electron microscope (Zeiss Sigma HD, Jena, Germany) is used to characterize the morphology of materials and to obtain the energy dispersive spectra.

2.2 Fabrication of gold volumetric nanocylinders

The sample fabrication is conducted by UV nanoimprint lithography. First, a soft transparent polymer stamp is imprinted by a nickel master mold with volumetric nanocylinders at the temperature range between 110°C and 150°C and under a pressure of 40 bar. Second, a silicon substrate spin-coated by a UV resist layer is imprinted by the stamp at a temperature of 65°C and under a pressure of 30 bar. Third, the substrate is subjected to UV exposure and oxygen plasma etching. Finally, a 5 nm chromium layer and a gold layer of about 250 nm are deposited on the substrate.

2.3 Loading of PS nanospheres

The substrates with the gold volumetric nanocylinders are processed by the nanosphere lithography for the loading of PS nanospheres, as shown in Figure 2. In the beginning, a 50.8 mm (in diameter) silicon wafer is immersed

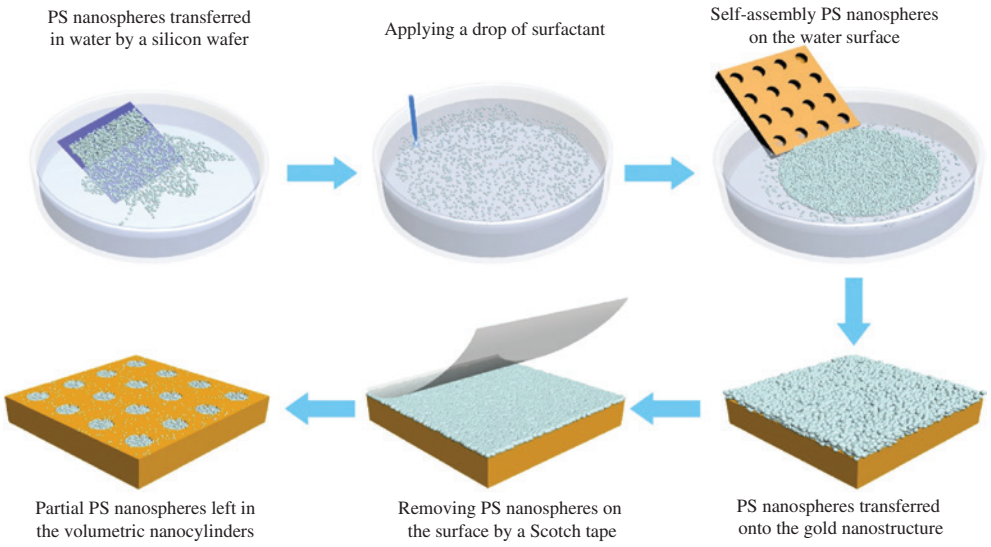

Figure 2: Process flow chart for loading nanoscale volume clusters of PS nanospheres in the volumetric nanocylinders.

in 10%*wt* sodium dodecyl sulfate (SDS) solution for more than 24 h to improve its surface hydrophilicity. The wafer is taken out and rinsed with deionized water. After that, a drop of 100 ~ 200 µl PS nanosphere suspension is applied on the wafer, and the wafer is shaken slowly and carefully in order to make the droplet spread evenly on its surface. The wafer is inserted into a vessel of deionized water slowly and steadily at an inclined angle of about 45 degrees. The PS nanospheres self-assemble on the top surface of the water with a relatively loose distribution. A drop of 3%*wt* SDS solution is applied to accelerate the self-assembly speed and make the distribution of nanospheres much more compact. The substrate with the plasmonic nanostructure is slowly inserted into the water and used to transfer the self-assembled nanospheres by a series of slow and careful pulling operations. The substrate is then placed on a piece of filter paper for natural drying within 1 ~ 2 h. The substrate surface is repeatedly bonded with the Scotch tape until the PS nanospheres on the surface are thoroughly removed.

2.4 Loading and etching of paraffin

In this process, the substrate with the gold nanostructure is dipped into the liquated paraffin and kept at 45°C for 5 min. After that, the substrate is taken out smoothly and put on a hot plate at the temperature of 45°C. The nanostructure surface is wiped using a piece of lens wiping paper repeatedly. In order to maintain the liquid state of paraffin for the corresponding optical measurement, the substrate is kept on the hot plate. After that, the substrate is cooled down to the room temperature (25°C) for the optical measurement of the solid state paraffin. Next, the substrate is etched for 15 s by the inductively coupled oxygen plasma with 10% CF_4 at the power of 40 W, and then prepared for the following optical measurement.

2.5 Optical measurement and numerical simulation

A set of optical fiber probes in combination with a UV-visible spectrometer (Avantes BV, Apeldoorn, The Netherlands) are used to measure the optical spectra of all the samples. For normal incidence, we adopt a reflection fiber probe, which consists of six lighting fibers and one reading fiber (200 µm core) with an operational range from 250 nm to 1100 nm. For the oblique incidence, we use a transmitting fiber and a receiving fiber with the same incident and reflective angles. In optical measurements, the reflectance from a silver mirror is used as a spectral reference. The full-wave finite element method is used for the optical simulation of the proposed plasmonic structures. The illuminated area is large enough, so that we can adopt infinite unit cells with Floquet periodic boundary conditions in the simulation. The optical constants of gold can be obtained from the literature [18]. The refractive index of water, liquated paraffin and solid paraffin are 1.33, 1.48 and 1.52, respectively. Adaptive inhomogeneous tetrahedral mesh is adopted to discretize the unit cell, and the minimum edge length of the mesh element is as small as 0.5 nm to ensure the convergence and reproducibility of the simulation.

3 Results and discussion

3.1 Determining the size of the measuring tool

Generally, we can interpret the light-matter interaction for the plasmonic nanostructure without the specimen by the Bragg's coupling theory. With the light at an incident angle of θ, the resonant wavelength can be expressed by the following equation [19, 20],

$$\lambda = \frac{P}{\sqrt{m^2+n^2}}\left(\sqrt{\varepsilon_d \varepsilon_{Au}/(\varepsilon_d+\varepsilon_{Au})}+\sin\theta\right) \quad (1)$$

where P, integers (m, n), ε_{Au} and ε_d represent the periodicity of nanocylinders, the resonance order of the plasmonic mode, the permittivity of gold, and the environmental permittivity surrounding the gold surface, respectively. For the normal incident light, θ equals zero. This coupling theory assumes an ideal lattice of volumetric nanocylinders with reciprocal vectors and provides an approximate estimation of plasmonic resonant wavelength for the periodic gold nanostructure. However, this theory neglects the size effects of nanocylinders [21, 22]. For the purpose of measurement, we need to further focus on the size effects of nanocylinders on the optical response. In order to confirm the feasible size of the nanostructure, we perform a series of electromagnetic simulation and investigate the size effects on the optical reflectance, as shown in Figure 3. It is observed from Figure 3A that there is no distinct plasmonic resonance feature when the radius R is fixed at 125 nm and the depth D is smaller than 49 nm. This result implies when D is small enough, the gold nanostructure tends to be analogous to a flat gold film and there are no sufficient lattice reciprocal vectors to excite surface plasmon polaritons (SPPs) efficiently. As D becomes larger than 49 nm, there is an obvious reflectance dip due to the (1, 0) order of plasmonic resonance. The wavelength of such plasmonic resonance has a considerable red shift as D increases from 49 nm to 200 nm. While D is larger than 200 nm, the resonant wavelength is seldom changed. The reason is that the SPPs is an evanescent wave, it has an optical field decay

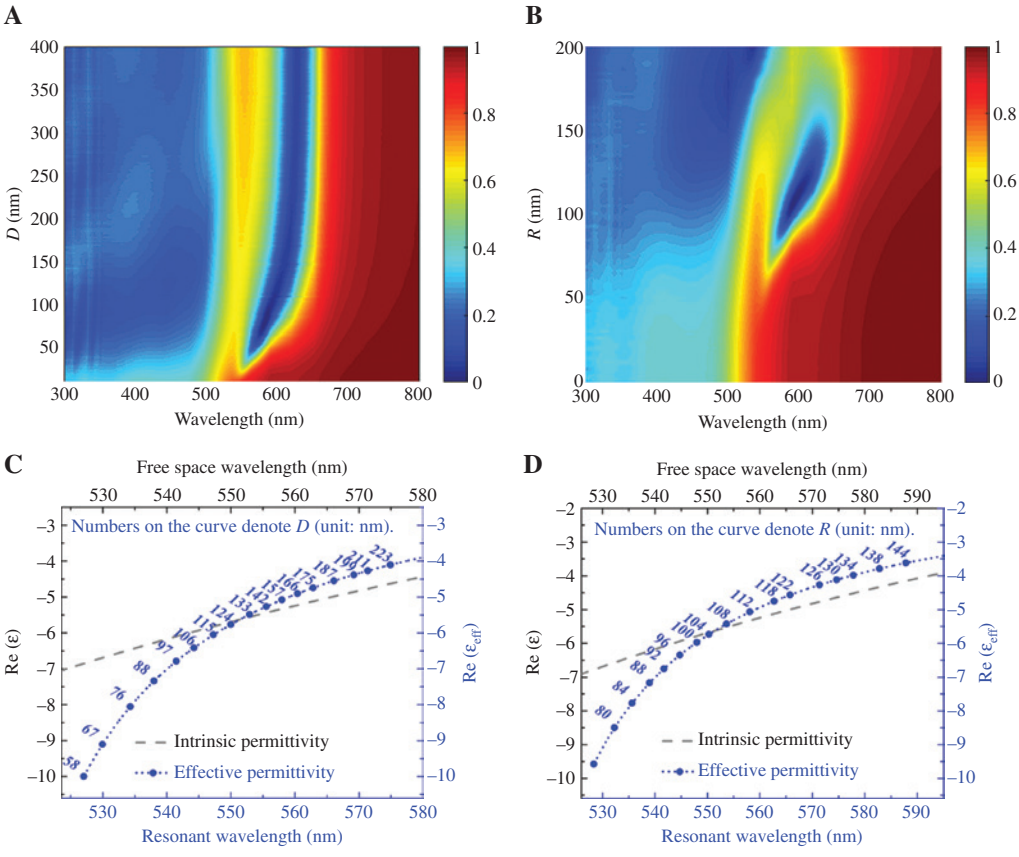

Figure 3: Reflectance spectra and resonant wavelengths for unloaded nanocylinders.
(A) Reflectance as a function of wavelength and D for $R = 125$ nm. (B) Reflectance as a function of wavelength and R for $D = 150$ nm. (C) Effective permittivity at the resonant wavelength for each value of D, when $R = 125$ nm. (D) Effective permittivity at the resonant wavelength for each value of R, when $D = 150$ nm.

length within the substrate consisting of gold and volumetric nanocylinders, and this field is significantly attenuated as D is increased to larger than 200 nm. Therefore, too shallow (less than 49 nm) volumetric nanocylinders are not feasible for the measurement due to the weak plasmonic excitation, and too deep (larger than 200 nm) ones are not necessary due to few influences from additional length effect and increased fabrication difficulties. Based on the above analysis, the best size choice of D for nanoscale volume measurement should be in the range from 49 nm and 200 nm. On the other hand, there is also a trade-off on determining the radius of the volumetric nanocylinders in order to obtain the optimized plasmonic effects for the measurement of nanoscale volumes. As shown in Figure 3B, when D is fixed at the value of 150 nm, the dramatic reflectance dip feature due to plasmonic resonance is only observed in the radius range from about 74 nm to 166 nm. When R is too small (e.g. less than 73 nm), there is no obvious plasmonic resonance feature. For R larger than 166 nm, the electromagnetic coupling between neighboring volumetric nanocylinders will broaden the resonance bandwidth and degrade the measurement effects because of a lower quality factor. According to Figure 3B, the optimized radius could be in the range from 90 nm to 146 nm. In order to have a better quantitative understanding of the size effect for Equation 1, we introduce the concept of equivalent permittivity for the combination of bulk gold and air nanocylinders, which is determined by various D and R. As observed from Figure 3C, the real part of effective permittivity $\mathrm{Re}(\varepsilon_{\mathrm{eff}})$ at the resonant wavelength for $D = 125$ nm is equal to the real part of intrinsic permittivity $\mathrm{Re}(\varepsilon)$ of bulk gold. As D is reduced, $\mathrm{Re}(\varepsilon_{\mathrm{eff}})$ for the corresponding resonance decreases significantly. In contrast, as D is increased, this value becomes larger with the change rate smaller and smaller. The similar optical properties can be found in Figure 3D, in which $\mathrm{Re}(\varepsilon_{\mathrm{eff}})$ is equal to $\mathrm{Re}(\varepsilon)$ for $R = 106$ nm. Based on the above analysis, the selection of appropriate nanoscale containers is critical for performing the measurement and the nanoscale measuring containers can be optimized by tuning the size of the nanostructures.

3.2 Measuring functionality by theoretical perspective

Based on above analysis and optimization of unloaded plasmonic nanostructures, we select the depth D of 200 nm and the radius R of 125 nm and fix the periodicity at 500 nm for further evaluation of the measuring functionality. To reveal the physical insight of the proposed method, we first assume a representative material to be measured (e.g. water with a refractive index of ~1.33) and adopt a simplified model neglecting the influence of liquid surface tension. We perform a series of optical simulations under normal incidence and investigate the reflectance spectra for the unloaded nanostructure ($H = 0$ nm), the partially-loaded nanostructure ($H = 120$ nm), the fully-loaded nanostructure ($H = 200$ nm), and the nanostructure totally immersed in the water environment, as shown in Figure 4A. There is an obvious reflectance dip at the wavelength of 569 nm, which is attributed to the (1, 0) order plasmonic resonance. When the nanoscale volume of $\pi \times 125\ \mathrm{nm}^2 \times 120$ nm is loaded to each plasmonic volumetric nanocylinder, the reflectance dip shifts to the wavelength of 613 nm. As the plasmonic volumetric nanocylinders are filled with nanoscale volumes, the reflectance dip shifts to the wavelength of 674 nm. This indicates that a given resonance wavelength corresponds to the specific nanoscale water inside the nanocylinder. Through the offset of the resonance wavelength, one can read out the volume value if the refractive index is known. When the plasmonic nanostructure is entirely immersed in water, we find that there are two reflectance dips, which is attributed to the (1, 0) order and the high-order plasmonic resonances, respectively. The (1, 0) order resonance shifts to 748 nm and the trend for the red shift is consistent with the other cases ($H = 120$ nm and $H = 200$ nm) in Figure 4A. In particular, the high order mode is not observed for H equals to 0 nm, 120 nm or 200 nm in the wavelength range from 300 nm to 800 nm. This is because there is inherent strong optical energy dissipation in gold for the wavelengths below 525 nm [23]. Due to the material optical property limitation of gold, the high order resonance modes for $\lambda < 525$ nm are not excited effectively for the cases of $H = 0$ nm, $H = 120$ nm and $H = 200$ nm. In contrast, the high order mode for the nanostructure in water exists in the wavelength range above 525 nm, so it can be excited normally. By virtue of the differences, one can discriminate whether the water overflows the volumetric nanocylinders by observing if there is an additional resonance mode for the gold nanostructure in the visible range. Furthermore, we reveal the light-matter interaction mechanisms by comparing the electric field distributions for various cases, as shown in Figure 4B–I. When the nanocylinders are empty, the electric field intensity at the resonant wavelength of 569 nm increases gradually from the bottom to the mouth in the nanocylinder, and induces strong optical absorption in the upper edge of the nanocylinder, as shown in Figure 4B. The addition of water in the nanocylinder changes the electric field distribution as shown in Figure 4C–E. As the level of water increases, the electric field intensity at $\lambda = 569$ nm

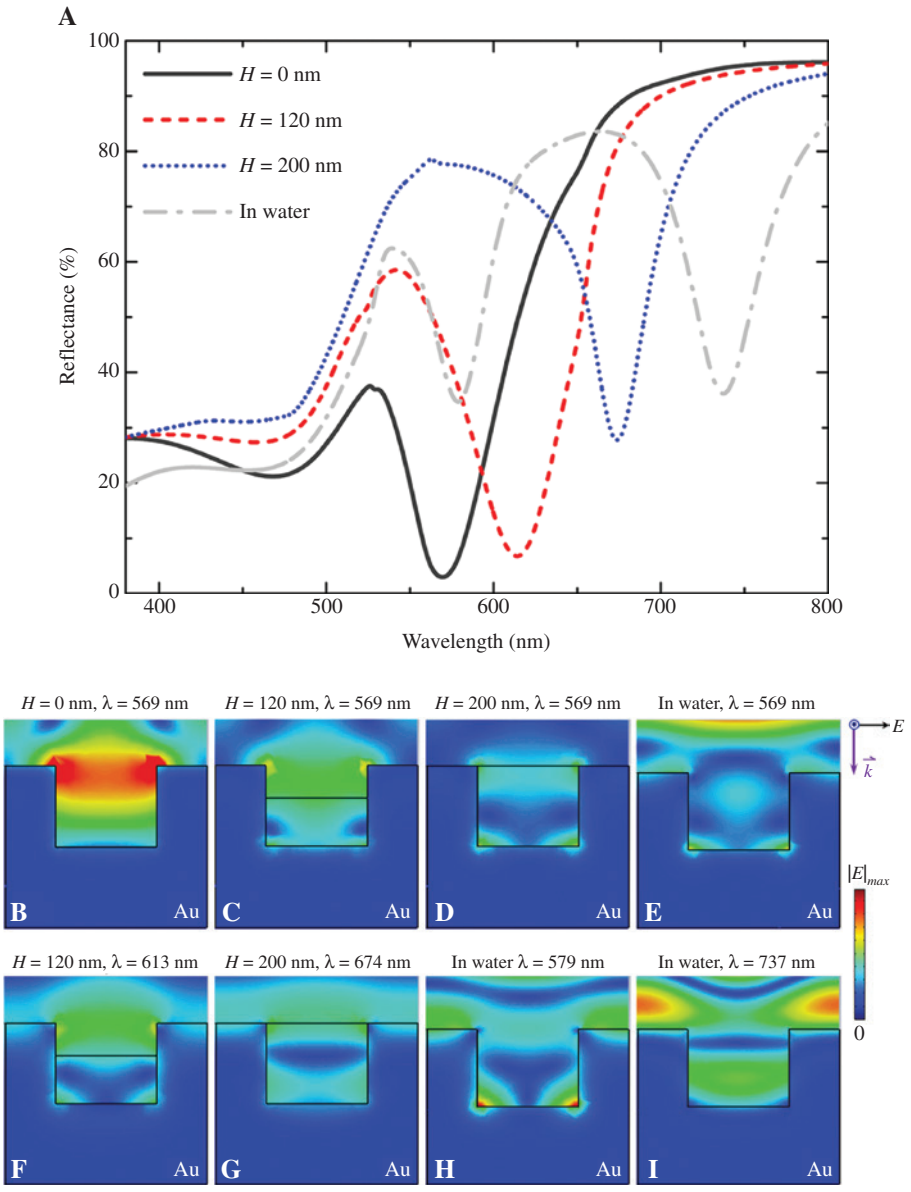

Figure 4: Optical spectra and electric field distributions for the changes of nanoscale volumes.
(A) Reflectance spectra for various values of *H* and for the immersion in water. Electric field distributions: (B–E) for various values of *H* and the immersion in water at $\lambda = 569$ nm, which is the resonance wavelength of the unloaded plasmonic nanostructure; (F) for $H = 120$ nm at the resonant wavelength of 613 nm; (G) for $H = 200$ nm at the resonance wavelength of 674 nm; (H) in water at the high order resonant wavelength of 579 nm; (I) in water at the low order resonant wavelength of 737 nm.

becomes smaller gradually, which can be observed from Figure 4B–D. As shown in Figure 4F and G, the electric field intensity at the corresponding resonant wavelength still has the maximum value surrounding the mouth of the nanocylinder, but it is reduced accordingly, which leads to less optical absorption (i.e. higher reflection) at the resonance position. This is consistent with the reflectance dips shown in Figure 3A. The nanostructure in water has two distinct resonant modes at $\lambda = 579$ nm and $\lambda = 737$ nm, which correspond to the enhanced field at the bottom of the nanocylinder and on top of the nanocylinder, respectively. The series of optical simulations provide the comprehensive understanding and guide for the experiments.

3.3 Characterization for nanofabrication and loading of nanoscale volumes

In order to validate the theoretical perspective, we perform nanoimprint lithography to fabricate the gold

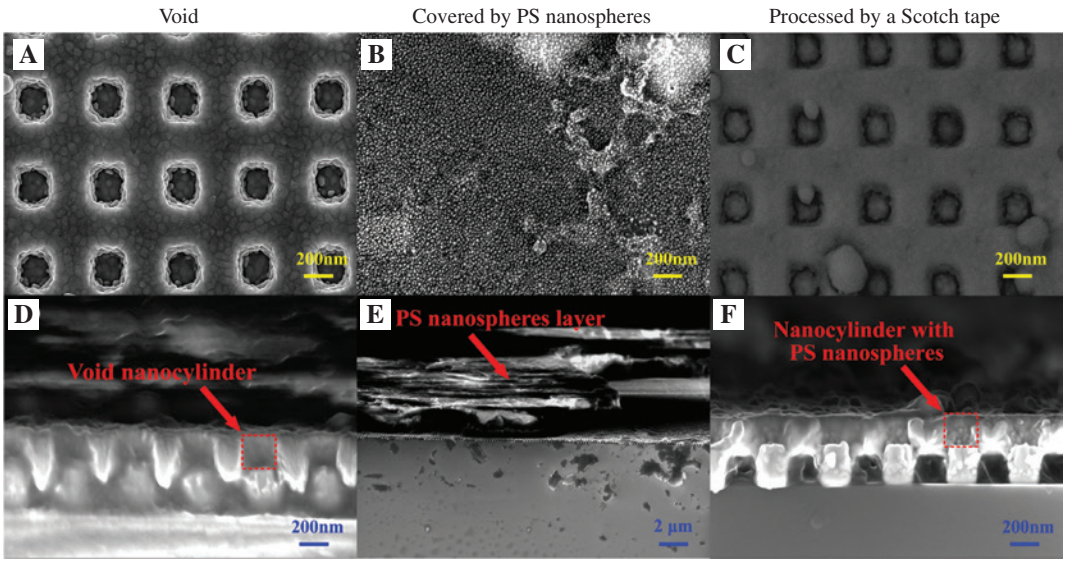

Figure 5: SEM images.
Top view: (A) uncovered gold nanostructure (Figure S1); (B) gold nanostructure covered by PS nanosphere layers (Figure S2); (C) gold volumetric nanocylinders loaded with PS nanospheres (Figure S3). Cross-section view: (D) uncovered gold nanostructure; (E) gold nanostructure partially covered by PS nanosphere layers; (F) gold volumetric nanocylinders loaded with PS nanospheres.

nanocylinders to achieve the measuring functionality in experiments. In practice, the use of nanoscale water is still a challenge due to the nanostructure surface tension effects. In view of this, we use the soft materials (such as PS nanospheres and paraffin) instead, which are relatively easier to be experimentally loaded at the nanoscale. Here, we load nanoscale volumes of PS nanospheres by the transfer method [24]. As can be seen in Figure 5A, the void plasmonic nanocylinders have a clean surface without any loading of PS nanospheres. Such a surface indicates a uniform array of hollow volumetric nanocylinders, which demonstrates the relatively consistent shape and size as the previous design through theoretical simulation. The corresponding cross-section view in Figure 5D further displays the uniform shape and size of the nanocylinders without any loading of PS nanospheres. Besides, Figure 5D indicates that the nanocylinders are formed on top of the patterned polymer resist generated in the nanoimprint process. After the transfer of PS nanospheres by virtue of the use of water, there are full of PS nanospheres on top of the plasmonic structure surface, as shown in Figure 5B. These PS nanospheres have a diameter of about 30 nm, and show the multiple stacked monolayers by the effect of self-assembly as observed in the cross-section in Figure 5E. The PS nanosphere layers have a thickness of about 0.8 μm with a certain surface roughness on the top. After removing most of the PS nanospheres using a Scotch tape, we can mainly keep clusters of PS nanospheres inside the nanocylinders, as shown in Figure 5C and F. It can be observed in Figure 5C, that most of the PS nanospheres are taken away using the Scotch tape except for some small piecemeal clusters on the top surface. By comparing the surface roughness of Figure 5C and F with Figure 5A and D, we can confirm that an amount of PS nanospheres are loaded into the volumetric nanocylinders. Therefore, we can further perform optical measurement for the three samples shown in Figure 5, in order to verify our theoretical assumption. In addition, the volumetric nanocylinders are also fully loaded with liquated paraffin for further evaluation by optical measurements.

3.4 Spectral measurement and analysis

Based on the experiments, we measure and compare the spectra for the experimental samples. As shown in Figure 6A, the addition of PS nanosphere clusters in the nanocylinders induces an obvious red shift of the plasmonic resonance wavelength from about 570 nm to about 585 nm due to the change of local refractive index inside the nanocylinders, and this property is consistent with the result shown in Figure 4A, which experimentally confirms the measuring functionality of the proposed plasmonic nanostructure. If we transfer a layer with sparse PS nanosphere clusters from the water surface, there is also a red shift from about 570 nm to about 579 nm, but the entire reflectance is reduced more significantly and the plasmonic resonance bandwidth is extremely broadened, compared

with the case with PS nanospheres included in the nanocylinders. By comparing the reflectance spectra, we can discriminate these two cases very clearly. It is observed that there are two resonance dips in the spectra for two other cases. One is that the nanostructure totally immersed in water has two resonance dips at 611 nm and 718 nm, respectively. Another is that the nanostructure covered with stacked PS nanosphere layers has two resonance dips at 624 nm and 731 nm, respectively. The resonance positions for the sample in water are consistent with the simulation result in Figure 4A except for small deviations and entirely lower reflectance. Such differences might be due to the practical variance of nanostructure shape and optical loss in water compared with the simulation model. Compared with the sample in water, the one covered by PS nanosphere layers has an obvious red shift. This could be attributed to the larger effective refractive index of PS nanosphere layers than the refractive index of water (~1.33). A simple optical simulation is provided for a better physical understanding in Figure S4 of the Supplementary Information. In addition, the entire reflectance for the sample with PS nanosphere layers is much lower, which is attributed to the stronger scattering and attenuation by the stacked layers of PS nanospheres. As demonstrated in the above theoretical analysis, the observation of the reflective spectral change from two resonance dips to one resonance dip is a critical clue to determine if the applied Scotch tape removes the PS nanospheres on the top surface thoroughly. To further demonstrate the nanoscale measuring functionality, we compare the spectra for the void nanocylinders and the nanocylinders including various nanoscale volumes of paraffin through experiments, as shown in Figure 6B. The full loading of liquated paraffin makes the resonance wavelength shifts from about 569 nm to about 715 nm, which reveals the similar spectral change as the simulation demonstrates in Figure 4. As the environmental temperature is reduced from 45°C to 25°C, the resonance dip has a blue shift to 689 nm, as shown in Figure 6B. The refractive index of the solid paraffin is slightly higher than that of the liquid paraffin (1.52 vs. 1.48), but the increase of the refractive index does not bring about a red shift. This is because the phase of paraffin changing from the liquid to the solid also makes the nanoscale volume shrunken by about 11% in each nanocylinder, which would considerably reduce the nanoscale height H from 200 nm to 178 nm and lead to the obvious blue shift as shown in Figure 6B. The experimental results indicates good consistency with the full wave optical simulation. In experiments, the plasmonic resonance shows a larger bandwidth and a lower quality factor than in simulations, which might be due to the slight inhomogeneity and the optical loss of paraffin

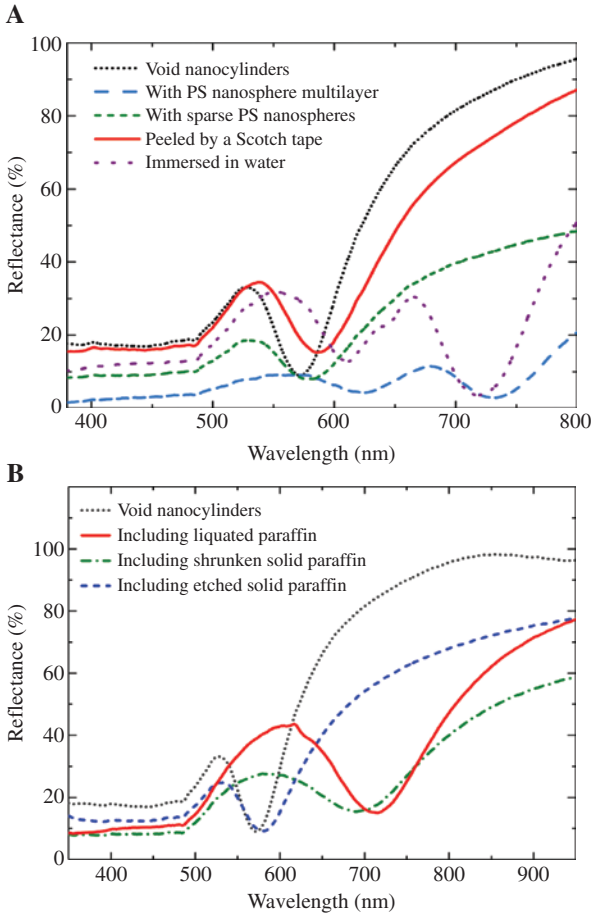

Figure 6: Measured optical reflectance for various samples. (A) Processed by the nanosphere lithography technique. (B) Processed by using paraffin loading and etching (Figure S5).

in each nanocylinder that is not considered in the ideal simulation model. Nevertheless, the shift for the central wavelength of resonance can statistically illuminate the nanoscale volume change of paraffin in the plasmonic nanocylinders, which is absolutely sufficient for the volume measurement of many kinds of nanomaterials. Furthermore, as observed from Figure 6B, when the nanoscale solid paraffin is partially reduced by plasma etching, the plasmonic resonance dip has a dramatic blue shift to the wavelength of about 581 nm, by which we could calculate that the height H for the etched nanoscale paraffin is about 30 nm in virtue of the optical simulation results.

3.5 Improvement of measuring performance

In order to improve the nanoscale measuring functionality, one could manipulate the incident angle of light for better performance [17]. Here, we define the figure of merit

(FOM) for the measuring nanostructure as expressed below,

$$\mathrm{FOM} = \frac{\Delta\lambda}{\mathrm{FWHM}} f(V) \tag{2}$$

where $\Delta\lambda$ denotes the wavelength shift from the void state to the loaded state with the nanoscale volumes of materials, and $f(V)$ is a function of the nanoscale volume V in each nanocylinder. It is worth mentioning that the full wave at half maximum (FWHM) can be usually increased by using a larger unit period under normal incidence due to the increase of resonance wavelength. Here, we fix the nanostructure and focus on investigating the influence of incident angle. Although the resonance wavelength under oblique incidence is increased, the FWHM is reduced significantly due to the angular manipulation, the result of which is consistent with the previous research work in [19]. As shown in Figure 7, by increasing the incident angle for an unpolarized light, the plasmonic resonance FWHM for the (1, 0) order can be significantly reduced, and the quality factor and the measuring sensitivity can be remarkably enhanced in comparison with the results for normal incidence (shown in Figure 6A). As shown in Figure 7B, at an incident angle of 60°, the empty nanocylinders and the ones loaded by PS nanospheres with a given nanoscale volume V_1 can be clearly distinguished by the resonance wavelength from 781.5 nm to 862.5 nm. These results indicate a red shift of about 81 nm and an FWHM of about 22.1 nm, and the FOM is $3.67f(V_1)$, which is 13 times more than the FOM of $0.28f(V_1)$ for the measurement under normal incidence. These results also reveal that tuning the incident angle of light introduces one more degree of manipulation freedom on improving the measurement performance for nanoscale volumes of materials.

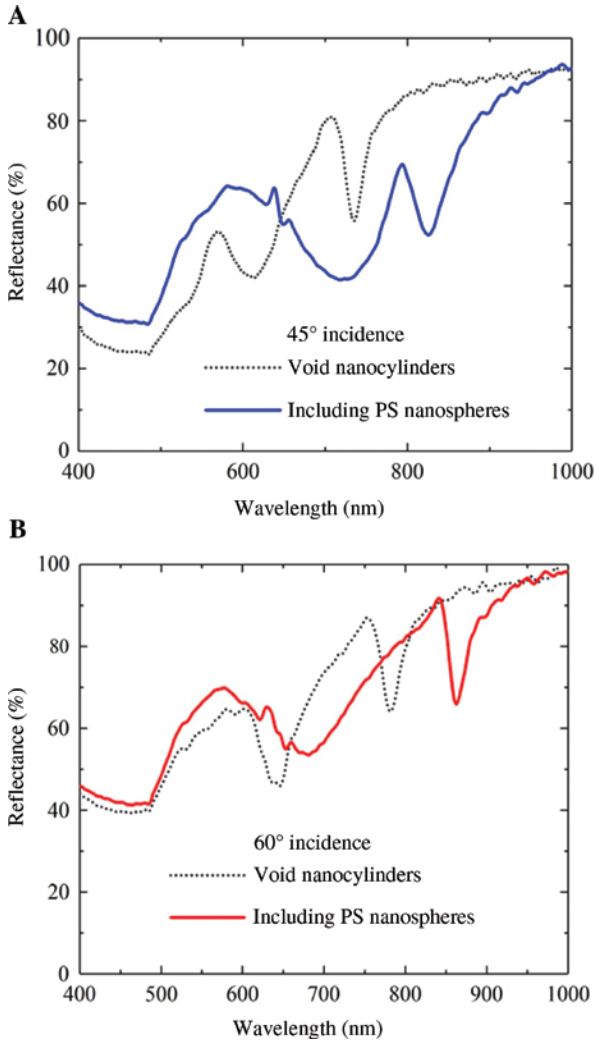

Figure 7: Measured optical reflectance for the samples with and without PS nanospheres under two different incident angles. (A) 45°. (B) 60°.

4 Conclusions

In summary, we have introduced a plasmonic analog of the graduated cylinders for the nanoscale volume measurement of materials. We have demonstrated the concept by the comprehensive numerical analysis, and experimentally revealed the potential applications of plasmonic containers through evaluating the spectral change by loading PS nanosphere clusters and nanoscale volumes of paraffin. Our method paves the way for fast non-destructive measurement of nanomaterials, and it will benefit many nanotechnology-related fields including in situ observation of biomolecules, biomedical sensing, integrated circuit technology and chemical analysis at the nanoscale. In future work, the nanostructure surface modification and nanoscale liquid tension could be further investigated for better understanding of the nanoscale liquid measurement and comprehensive applications.

Acknowledgments: This work was supported by NSAF (Grant No. U1830116); Natural Science Foundation of Guangdong Province (Grant No. 2018A030313299, Funder Id: http://dx.doi.org/10.13039/501100003453); Fujian Provincial Department of Science and Technology (Grant No. 2017J01123, Funder Id: http://dx.doi.org/10.13039/501100005270); the Fundamental Research Funds for the Central Universities (Grant No. 20720190010); the fund of Key Laboratory of THz Technology, Ministry of Education, China.

References

[1] Yoo WC, Kumar S, Penn RL, et al. Growth patterns and shape development of zeolite nanocrystals in confined syntheses. J Am Chem Soc 2009;34:12377–83.

[2] Liu J, Huang Y, Kumar A, et al. pH-sensitive nano-systems for drug delivery in cancer therapy. Biotechnol Adv 2014;4:693–710.

[3] Herda LM, Hristov DR, Lo Giudice MC, et al. Mapping of molecular structure of the nanoscale surface in bionanoparticles. J Am Chem Soc 2016;1:111–4.

[4] Gramse G, Dols-Pérez A, Edwards MA, et al. Nanoscale measurement of the dielectric constant of supported lipid bilayers in aqueous solutions with electrostatic force microscopy. Biophys J 2013;6:1257–62.

[5] Jiang L. Precision grating for measuring microscope lens distortions. Int J Metrol Qual Eng 2010;2:83–8.

[6] Li Y, Xu J, Li D. Molecular dynamics simulation of nanoscale liquid flows. Microfluid Nanofluid 2010;6:1011–31.

[7] Weber MS, Wojtynek M, Medalia O. Cellular and structural studies of eukaryotic cells by cryo-electron tomography. Cells 2019;1:57.

[8] Jackman JA, Ferhan AR, Cho NJ. Nanoplasmonic sensors for biointerfacial science. Chem Soc Rev 2017;12:3615–60.

[9] Park E, Campbell EB, MacKinnon R. Structure of a CLC chloride ion channel by cryo-electron microscopy. Nature 2017;7638:500.

[10] Ruozi B, Belletti D, Tombesi A, et al. AFM, ESEM, TEM, and CLSM in liposomal characterization: a comparative study. Internat J Nanomed 2011;6:557.

[11] Liu N, Hentschel M, Weiss T, et al. Three-dimensional plasmon rulers. Science 2011;6036:1407–10.

[12] Teperik TV, Nordlander P, Aizpurua J, et al. Robust subnanometric plasmon ruler by rescaling of the nonlocal optical response. Phys Rev Lett 2013;26:263901.

[13] Hill RT, Mock JJ, Hucknall A, et al. Plasmon ruler with angstrom length resolution. ACS Nano 2012;10:9237–46.

[14] Dathe A, Ziegler M, Hübner U, et al. Electrically excited plasmonic nanoruler for biomolecule detection. Nano Lett 2016;9:5728–36.

[15] Li CY, Le JB, Wang YH, et al. In situ probing electrified interfacial water structures at atomically flat surfaces. Nat Mater 2019;18:697–701.

[16] Zhu W, Esteban R, Borisov AG, et al. Quantum mechanical effects in plasmonic structures with subnanometre gaps. Nat Commun 2016;7:1149511508.

[17] Tan SF, Wu L, Yang JKW, et al. Quantum plasmon resonances controlled by molecular tunnel junctions. Science 2014;6178:1496–9.

[18] Palik ED. Handbook of optical constants of solids. San Diego, CA, USA, Academic Press, 1998.

[19] Liu B, Chen S, Zhang J, et al. A plasmonic sensor array with ultrahigh figures of merit and resonance linewidths down to 3 nm. Adv Mater 2018;12:706031–7.

[20] Zhu J, Bai Y, Zhang L, et al. Large-scale uniform silver nanocave array for visible light refractive index sensing using soft UV nanoimprint. IEEE Photonics J 2016;4:1–7.

[21] Zhou J, Tao F, Zhu J, et al. Portable tumor biosensing of serum by plasmonic biochips in combination with nanoimprint and microfluidics. Nanophotonics 2018;8:1–10.

[22] Cetin AE, Etezadi D, Galarreta BC, et al. Plasmonic nanohole arrays on a robust hybrid substrate for highly sensitive label-free biosensing. ACS Photonics 2015;8:1167–74.

[23] Zhu J, Zhang L, Bai Y, et al. Simultaneous fabrication of two kinds of plasmonic crystals by one nanoimprint mold. IEEE Photonics Technol Lett 2017;6:504–6.

[24] Zhu J, Zhu X, Hoekstra R, et al. Metallic nanomesh electrodes with controllable optical properties for organic solar cells. Appl Phys Lett 2012;14:143109–13.

Supplementary Material: The online version of this article offers supplementary material (https://doi.org/10.1515/nanoph-2019-0369).